MODELLING SIEVE TRAY HYDRAULICS USING COMPUTATIONAL FLUID DYNAMICS

R. KRISHNA and J. M. VAN BATEN

Department of Chemical Engineering, University of Amsterdam, Amsterdam, The Netherlands

The ability of computational fluid dynamics (CFD) to model the complex two-phase hydrodynamics of sieve trays is examined. The key to a proper description of the flow is the estimation of the momentum exchange, or drag, coefficient between the gas and liquid phases. In the absence of sound theoretical models, empirical correlations for the average gas fraction on the tray, such as those of Bennet, Agrawal and Cook [*AIChE J*, 29 (1983): 434], can be used to estimate the drag coefficient. Transient simulations of sieve trays of 0.3 and 0.9 m in diameter, operating in the bubbly flow regime, reveal the chaotic, three-dimensional character of the flow and the existence of circulation patterns in all three dimensions. The CFD simulations underline the limitations of simpler approaches wherein the flow is assumed to be two-dimensional or where the interaction of the liquid phase with the gas phase is either ignored completely or simplified greatly. The major advantage of the CFD approach is that geometry and scale effects are properly encapsulated and do not require further inputs. It is concluded that CFD can be a powerful investigative and design tool for sieve tray columns.

Keywords: computational fluid dynamics; sieve trays; clear liquid height; froth height; froth density; scale effects; liquid circulations.

INTRODUCTION

Distillation is the most widely used separation technique and is usually the first choice for separating mixtures. Only when distillation fails does one look for other separation alternatives. One of the major factors that favours distillation is the fact that large-diameter columns can be designed and built with confidence. Sieve tray distillation columns are widely used in industrial practice and the description of the hydrodynamics of sieve trays is of great importance. A proper prediction of the sieve tray hydraulics is necessary for the prediction of separation efficiency and overall tray performance. For a given set of operating conditions (gas and liquid loads), tray geometry (column diameter, weir height, weir length, diameter of holes, fractional hole area, active bubbling area, downcomer area) and system properties, it is necessary to predict the flow regime prevailing on the tray, liquid hold-up, clear liquid height, froth density, interfacial area, pressure drop, liquid entrainment, gas and liquid phase residence time distributions and the mass transfer coefficients in either fluid phase. A lack of in-depth understanding of the processes occurring within a distillation column is a significant barrier to the further improvement of equipment performance. In 1986, in the preface to his influential book, Lockett (1986) wrote 'Sieve tray decks are, after all, hardly more than sheets of metal with a few holes punched in them. This of course is part of the fascination—that the behaviour of something so simple can be so difficult to predict with regards to its hydrodynamic and mass transfer performance.' Design of sieve tray distillation columns is essentially empirical in

nature (Kister, 1992; Lockett, 1986; Stichlmair and Fair, 1998; Zuiderweg, 1982).

In recent years, there has been considerable academic and industrial interest in the use of computational fluid dynamics (CFD) to model two-phase flows in process equipment (Krishna and Van Baten, 2001a). CFD techniques have been used to model bubble formation and rise in liquids and powders (Krishna and Van Baten, 1999; Krishna et al., 2000a) and to describe the hydrodynamics of bubble columns (Borchersger et al., 1999; Krishna et al., 2000b) and fluidised beds (Krishna and Van Baten, 2001b; Van Wachem et al., 2001). An important advantage of CFD techniques is that geometry and scale effects are 'automatically' accounted for (Krishna et al., 2000b; Krishna and Van Baten, 2001a).

There have been some recent attempts to model sieve tray hydrodynamics using CFD (Liu et al., 2000; Krishna et al., 1999; Mehta et al., 1998; Van Baten and Krishna, 2000; Van Baten et al., 2001a,b). Mehta et al. (1998) analysed the liquid phase flow patterns on a sieve tray by solving the time-averaged equations of continuity of mass and momentum only for the liquid phase. Interactions with the vapour phase are taken account of by use of interphase momentum transfer coefficients determined from empirical correlations. Liu et al. (2000) attempt to model the two-phase flow behaviour using a two-dimensional model, focussing on the description of the hydrodynamics along the liquid flow path, ignoring the variations in the direction of gas flow along the height of the dispersion. Van Baten et al. (Van Baten and Krishna, 2000; Van Baten et al., 2001a,b) use

fully three-dimensional transient simulations to describe the hydrodynamics of sieve trays.

The objective of the present communication is to examine the power, and limitations of CFD techniques in describing sieve tray hydraulics. We review and extend our previous CFD approach (Krishna *et al.*, 1999; Van Baten and Krishna, 2000; Van Baten *et al.*, 2001a,b) to the description of liquid phase residence time distribution (RTD) and the influence of scale effects. We begin with a two-dimensional analysis of liquid phase channelling and bypassing on a tray.

TWO-DIMENSIONAL CFD ANALYSIS OF LIQUID PHASE CHANNELLING

Before attempting to model the complex gas–liquid tray hydrodynamics, let us consider CFD simulation of a simple case of flow of liquid across a round tray with the dimensions specified in Figure 1(a). A total of $48 \times 60 = 2880$ grid cells of warped configuration are used to cover the tray geometry. The liquid load per unit weir length is taken to be $8.25 \times 10^{-4} \, \mathrm{m^3 \, s^{-1} \, m^{-1}}$, corresponding to an inlet liquid velocity of $0.055 \, \mathrm{m \, s^{-1}}$. The mass and momentum conservation equations are:

$$\frac{\partial \rho_L}{\partial t} + \nabla \cdot (\rho_L \mathbf{u}_L) = 0 \tag{1}$$

$$\frac{\partial \rho_L \mathbf{u}_L}{\partial t} + \nabla \cdot \left\{ \rho_L \mathbf{u}_L \mathbf{u}_L - \mu_L [\nabla \mathbf{u}_L + (\nabla \mathbf{u}_L)^T] \right\}$$
$$= -\nabla p + \rho_L \mathbf{g} \tag{2}$$

where ρ_L, $\mathbf{u}_L$ and μ_L represent, respectively, the macroscopic density, velocity and viscosity of the liquid phase, p is the pressure, and $\mathbf{g}$ is the gravitational acceleration. The turbulent contribution to the stress tensor is evaluated by means of low Reynolds number variant of the k–ε model (Launder and Sharma, 1974), using standard single-phase parameters $C_\mu = 0.09$, $C_{1\varepsilon} = 1.44$, $C_{2\varepsilon} = 1.92$, $\sigma_k = 1$ and $\sigma_\varepsilon = 1.3$.

A commercial CFD package CFX 4.2 of AEA Technology, Harwell, UK, was used to solve equations (1) and (2) of continuity and momentum. This package is a finite volume solver, using body-fitted grids. Discretization of the equations at the grid is performed using a finite differencing (finite volume) method. Physical space is mapped to a rectangular computational space. Velocity vector equations are treated as scalar equations, one scalar equation for each velocity component. All scalar variables are discretised and evaluated at the cell centres. Velocities required at the cell faces are evaluated by applying an improved Rhie and Chow (1983) interpolation algorithm. Transport variables such as diffusion coefficients and effective viscosities are evaluated and stored at the cell faces. The pressure–velocity coupling is obtained using the SIMPLEC algorithm (Van Doormal and Raithby, 1984). For the convective terms in equations (1) and (2), hybrid differencing was used. The transient equations were solved with 0.01 s time steps until steady state was reached. A fully implicit backward differencing scheme was used for the time integration.

The steady-state velocity profiles are shown in Figure 1(b). The recirculation patterns in the rounded segments of the tray are evident. Such recirculation patterns were first highlighted in the classic paper of Porter *et al.* (1972). We note from Figure 1(b) that the liquid velocity in the central flow path is about $0.06 \, \mathrm{m \, s^{-1}}$, whereas the liquid is practi-

cally at a standstill in a major portion of rounded segments. CFD simulations can also be used to determine the residence time distribution by injecting a pulse tracer and monitoring its progression as it moves through the tray. Snapshots of the tracer movement are shown in Figure 2. It is clearly seen that, while the tracer concentration has reduced to practically zero in the central rectangular region within 8 s of tracer injection, it is swished to the rounded segmental regions and lingers there for a very long time. The normalized RTD is shown in Figure 3. The tracer response cannot be described by an axial dispersion model; on the other hand a model with N stirred tanks in series, exchanging tracer with a dead space, is able to match the tracer response very well; see the continuous lines in Figure 3. The best fit with the CFD simulations is obtained taking the number of stirred tanks $N = 40$ and the dead space volume to be 28% of the total tray volume. The exchange between the active and the dead zone amounts to only 0.004 of the inlet flow. From geometry considerations, the rounded segmental portions are 32% of the total tray volume; this is in close agreement with the dead zone determined from CFD simulations.

There are clear limitations of the above analysis, assuming *two*-dimensional flow of only *liquid* across the tray. This is because the introduction of the gas phase will have a significant influence on the recirculation patterns. Furthermore, the gas–liquid hydrodynamics assumes a truly chaotic nature, as we shall see below.

THREE-DIMENSIONAL SIMULATION STRATEGY FOR GAS–LIQUID HYDRODYNAMICS

There are many flow regimes on sieve trays (Lockett, 1986), ranging from gas-dispersed bubbly flow regime to liquid-dispersed spray flow regime; see Figure 4. From a CFD point of view, the bubbly flow regime is much easier to describe and model than the spray flow regime because it is easier to model the gas–liquid drag which is much more uniform along the dispersion height. On the other hand, in the spray flow regime, the gas–liquid drag can be expected to vary significantly up the dispersion, making the modelling much more difficult. We therefore restrict ourselves to the description of the bubbly flow regime. The derivation of the basic equations for dispersed two-phase flows is discussed by Jakobsen *et al.* (1997) and here we present a summary. For either gas (subscript G) or liquid (subscript L) phases in the two-phase dispersion on the tray the volume-averaged mass and momentum conservation equations are given by:

$$\frac{\partial (\varepsilon_G \rho_G)}{\partial t} + \nabla \cdot (\rho_G \varepsilon_G \mathbf{u}_G) = 0 \tag{3}$$

$$\frac{\partial (\varepsilon_L \rho_L)}{\partial t} + \nabla \cdot (\rho_L \varepsilon_L \mathbf{u}_L) = 0 \tag{4}$$

$$\frac{\partial (\rho_G \varepsilon_G \mathbf{u}_G)}{\partial t} + \nabla \cdot \left\{ \rho_G \varepsilon_G \mathbf{u}_G \mathbf{u}_G - \mu_G \varepsilon_G [\nabla \mathbf{u}_G + (\nabla \mathbf{u}_G)^T] \right\}$$
$$= -\varepsilon_G \nabla p + \mathbf{M}_{G,L} + \rho_G \varepsilon_G \mathbf{g} \tag{5}$$

$$\frac{\partial (\rho_L \varepsilon_L \mathbf{u}_L)}{\partial t} + \nabla \cdot \left\{ \rho_L \varepsilon_L \mathbf{u}_L \mathbf{u}_L - \mu_L \varepsilon_L [\nabla \mathbf{u}_L + (\nabla \mathbf{u}_L)^T] \right\}$$
$$= -\varepsilon_L \nabla p - \mathbf{M}_{G,L} + \rho_L \varepsilon_L \mathbf{g} \tag{6}$$

where ρ_k, $\mathbf{u}_k$, ε_k and μ_k represent, respectively, the macroscopic density, velocity, volume fraction and viscosity of the phase k, p is the pressure, $\mathbf{M}_{G,L}$, the interphase momentum exchange between gas and liquid phases and $\mathbf{g}$ is the gravitational acceleration. The gas and liquid phases share the same pressure field, $p_G = p_L = p$. The added mass force has been ignored in the present analysis. Lift forces are also ignored in the present analysis because of the uncertainty in assigning values of the lift coefficients. For the continuous, liquid, phase, the turbulent contribution to the stress tensor is evaluated by means of k–ε model, using standard single-phase parameters. No turbulence model is used for calculating the velocity fields of the dispersed gas bubbles in the bubbly flow regime.

The interphase momentum exchange term is:

$$\mathbf{M}_{L,G} = \frac{3}{4}\rho_L \frac{\varepsilon_G}{d_G} C_D (\mathbf{u}_G - \mathbf{u}_L)|\mathbf{u}_G - \mathbf{u}_L| \qquad (7)$$

where C_D is the interphase momentum exchange coefficient or drag coefficient. The proper estimation of the drag coefficient is the key to the successful modelling of the tray hydraulics. For the Stokes regime:

$$C_D = 24/\mathrm{Re}_G; \quad \mathrm{Re}_G = \rho_L U_G d_G / \mu_L \qquad (8)$$

and for the inertial regime, also known as the turbulent regime:

$$C_D = 0.44 \qquad (9)$$

For the churn-turbulent regime of bubble column operation (Krishna *et al.*, 2000b; Krishna and Van Baten, 2001a) the drag coefficient for a swarm of large bubbles is estimated using:

$$C_D = \frac{4}{3}\frac{\rho_L - \rho_G}{\rho_L} g d_G \frac{1}{V_{\mathrm{slip}}^2} \qquad (10)$$

where V_{slip} is the slip velocity of the bubble swarm with respect to the liquid:

$$V_{\mathrm{slip}} = |\mathbf{u}_G - \mathbf{u}_L| \qquad (11)$$

Substituting equation (10) into equation (7) we find:

$$\mathbf{M}_{L,G} = \varepsilon_G (\rho_L - \rho_G) g \frac{1}{V_{\mathrm{slip}}^2} (\mathbf{u}_G - \mathbf{u}_L)|\mathbf{u}_G - \mathbf{u}_L| \qquad (12)$$

The slip between gas and liquid can be estimated from superficial gas velocity U_G and the gas hold-up ε_G:

$$V_{\mathrm{slip}} = U_G / \varepsilon_G \qquad (13)$$

An empirical correlation for the gas fraction on the tray as a function of the superficial gas velocity can be used to the estimate the slip velocity. In this work, we use the Bennett *et al.* (1983) correlation to estimate the gas hold-up:

$$\varepsilon_L^B = \exp\left[-12.55\left(U_G\sqrt{\frac{\rho_G}{\rho_L - \rho_G}}\right)^{0.91}\right]; \; \varepsilon_G^B = 1 - \varepsilon_L^B \qquad (14)$$

It is important to note that the Bennett correlation does not include tray geometry or scale parameters. The interphase momentum exchange term is therefore:

$$\mathbf{M}_{L,G} = \varepsilon_G (\rho_L - \rho_G) g \frac{1}{(U_G/\varepsilon_G^B)^2} (\mathbf{u}_G - \mathbf{u}_L)|\mathbf{u}_G - \mathbf{u}_L| \qquad (15)$$

This formulation, however, gives numerical difficulties because in the freeboard the liquid hold-up is zero. In order to overcome this problem we modify equation (15) as follows:

$$\mathbf{M}_{L,G} = \varepsilon_G \varepsilon_L (\rho_L - \rho_G) g \left[\frac{1}{(U_G/\varepsilon_G^B)^2}\frac{1}{\varepsilon_L^B}\right](\mathbf{u}_G - \mathbf{u}_L)|\mathbf{u}_G - \mathbf{u}_L| \qquad (16)$$

where the term

$$\left[\frac{1}{(U_G/\varepsilon_G^B)^2}\frac{1}{\varepsilon_L^B}\right]$$

is estimated *a priori* from the Bennett relation, equation (14), and the desired gas velocity. This approach ensures that the average gas hold-up in the gas–liquid dispersion on the froth conforms to experimental data over a wide range of conditions (as measured by Bennett *et al.*, 1983). When incorporating equation (16) for the gas–liquid momentum exchange within the momentum balance relations (5) and (6), the local transient, values of $\mathbf{u}_G$, $\mathbf{u}_L$, ε_G and ε_L are used. A further point to note is that use of equation (16) for the momentum exchange obviates the need for specifying the bubble size. Indeed, for the range of superficial gas velocities used in our simulations to be reported below, 0.5–$0.9\,\mathrm{m\,s}^{-1}$, we do not expect well-defined bubbles. The two-phase Eulerian simulation approach used here only requires that the gas phase is the dispersed phase; this dispersion could consist of either gas bubbles or gas jets, or a combination thereof.

Figure 5 shows the configuration of the system that has been simulated. The diameter of the tray is $0.3\,\mathrm{m}$ with a height of $0.12\,\mathrm{m}$. The length of the weir is $0.18\,\mathrm{m}$, giving a flow path length of $0.24\,\mathrm{m}$. The chosen height of $0.12\,\mathrm{m}$ is sufficient to prevent liquid carryover out of the computational space. The liquid enters the tray through a rectangular opening that is $0.015\,\mathrm{m}$ high. The height of the weir is varied in the simulations and has the values of 60, 80 and 100 mm. The total number of grid cells used in the simulations is $48 \times 60 \times 24 = 69,120$; 48 cells in liquid flow direction, 60 cells in direction perpendicular to the liquid flow and 24 cells in the vertical direction. Figure 6 shows the layout of the distributor grid, which consists of 180 holes. The choice of the grid size is based on our experience gained in the modelling of fluidized beds and gas–liquid bubble columns operating in the churn-turbulent regime (Krishna *et al.*, 2000b; Krishna and Van Baten, 2001a,b). The use of warped square holes does not impact on the simulation results, because we use the Eulerian framework for describing either fluid phase.

Air, at ambient pressure conditions, and water were used as the gas and liquid phases respectively. At the start of a simulation, the tray configuration shown in Figure 5 is filled with a uniform gas–liquid dispersion, with 10% gas holdup, up to the height of the weir and gas is injected through the holes at the distributor. The time increment used in the simulations is 0.002 s. During the simulation, the volume fraction of the liquid phase in the gas–liquid dispersion in the system is monitored and quasi-steady state is assumed to prevail if the value of the hold-up remains constant for a period long enough to determine the time-averaged values of the various parameters. For obtaining the values of the clear liquid height, gas holdup of dispersion, etc., the parameter values are averaged over a sufficiently long period over which the holdup remains steady.

Simulations have been performed on a Silicon Graphics Power Challenge with six R10000 processors running at 200 MHz. A typical simulation took about 4 days to simulate 20 s of tray hydrodynamics. From the simulation results, average liquid hold-up as a function of height has been determined. Clear liquid height has been determined by multiplying the average liquid hold-up with the height of the computational space (0.12 m). Further computational details of the algorithms used, boundary conditions, including animations are available on our web site (http://ct-cr4.chem. uva.nl/sievetrayCFD/).

Let us first consider snapshots, at 5 s intervals, of the movement of liquid along the flow path and over the weir; see Figures 7 and 8. Near the bottom of the tray, the liquid is drawn toward the centre and is dragged up vertically by the gas phase. The liquid disengages itself from the dispersed gas phase and travels down the sides, resulting in circulation cells that are evident in both the front (Figure 7) and weir (Figure 8) views. The snapshots also reflect the chaotic nature of the flow. There are two circulation cells when viewed from the front and from the weir.

Snapshots of the liquid flow patterns viewed 10 and 40 mm above the tray floor are shown in Figure 9. Near the bottom of the tray the liquid is drawn inward and carried upwards; this is evidenced by the fact that all the liquid velocity vectors are pointing inwards; see 10 mm view at the top of the Figure 9. Liquid recirculations are clearly visible in the 40 mm view at the bottom of Figure 9. The circulation patterns clearly have a chaotic character. When the transient simulations are time-averaged, the liquid phase velocity vectors at 40 mm above the tray are obtained as shown in Figure 10. The recirculation cells at the rounded segments are clearly seen. However, it is interesting to note that the liquid velocity is directed towards the centre; this is because of the circulation cells seen in the front and weir views in Figures 7 and 8 respectively. The liquid phase circulations *with gas flow* have therefore a totally different character than *without gas flow* (Figure 2).

Figure 11 presents typical simulation results for the variation of the liquid hold-up along the height of the dispersion. The values of the hold-up are obtained after averaging along the x- and y-directions and over a sufficiently long time interval once quasi-steady-state conditions are established. The simulated trends in liquid hold-up as a function of the gas velocity U_G are in line with literature information (Hofhuis and Zuiderweg, 1979).

Figure 12 (a)–(c) compares the calculations of the clear liquid height from CFD simulations with the Bennett *et al.* (1983) correlation:

$$h_{cl} = \varepsilon_L^B \left[h_w + C \left(\frac{Q_L}{W \varepsilon_L^B} \right)^{0.67} \right];$$
$$C = 0.50 + 0.438 \exp(-137.8 h_w) \tag{17}$$

where ε_L^B is determined from equation (14). It must be emphasized that equation (17) is entirely independent of the holdup correlation presented in equation (14). Put another way, the incoporation of the holdup correlation into our CFD inputs does not imply anything by way of information on the clear liquid height. The values of the clear liquid height from the simulations are obtained after averaging over a sufficiently long time interval once quasi-steady-state conditions are established and determining the cumulative liquid hold-up within the computational space. It is remarkable to note that the clear liquid height determined from the CFD simulations matches the Bennett correlation quite closely, even though no influence of the weir height or liquid weir load on the interface gas–liquid momentum exchange coefficient has been used in the model. Geometry effects are properly taken account of in the CFD approach.

We have also studied the residence time distribution (RTD) of liquid phase by following the course of a tracer (red colour) in the liquid entering at the inlet to the tray. In order to gain insight into the tracer movement in the liquid phase, let us consider a specific tray operation at $U_G = 0.7 \, \text{m s}^{-1}$, weir height $h_w = 80 \, \text{mm}$; liquid load $Q_L/W = 8.25 \times 10^{-4} \, \text{m}^3 \, \text{s}^{-1} \, \text{m}^{-1}$. Snapshots of the tracer concentrations at various time steps from start of the pulse tracer are shown in Figure 13. In sharp contrast to the corresponding two-dimensional liquid simulations shown in Figure 3, we note that there is no starvation of tracer at the segmental regions; the tracer appears to be dispersed over the whole tray cross section. Put another way, the chaotic gas–liquid hydrodynamics leads to good tracer dispersion.

The major advantage of CFD simulations is that scale effects are captured. In order to illustrate this, let us consider simulations of at 0.9 m diameter tray operating at $U_G = 0.7 \, \text{m s}^{-1}$, weir height $h_w = 80 \, \text{mm}$; liquid load $Q_L/W = 8.25 \times 10^{-4} \, \text{m}^3 \, \text{s}^{-1} \, \text{m}^{-1}$. A total of 622,080 cells are required to capture the hydrodynamics. A snapshot of the front view of the tray shows the existence of multiple cells, four in number, in the flow direction; see Figure 14(a). This is in sharp contrast to the 0.3 m diameter tray, which displayed only two circulation cells in the flow direction. The weir view of the tray also shows the existence of four circulation cells; see Figure 14(b).

When the 0.9 m tray is viewed from the top at a position 40 mm above the tray floor, we again note a multiplicity of circulation patterns; see Figure 15. It is clear that, as the column diameter increases, so do the number of circulation cells. This implies that the liquid phase will be more backmixed in columns of smaller diameter. The liquid phase in large diameter columns will approach plug flow character.

The time averaged clear liquid height, h_{cl}, for the 0.9 m tray after quasi-steady state has been achieved is almost identical to that of the 0.3 m diameter tray; the simulation results are compared in Figure 12. There is a small scale effect with regard to clear liquid height and gas holdup on
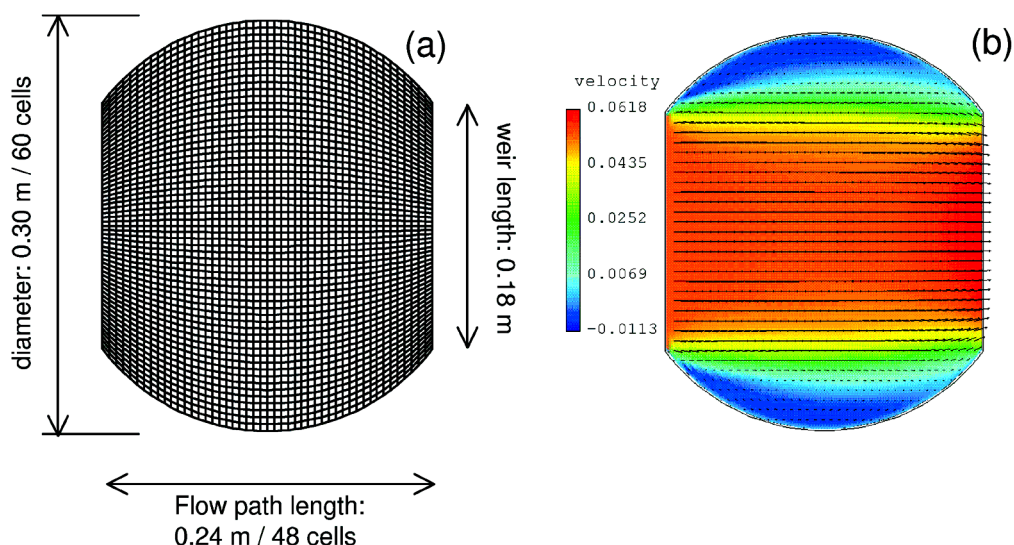
Figure 1. Two-dimensional simulation of liquid flow across a tray of 0.3 m diameter. (a) Computational grid. (b) Steady-state velocity profiles shown in colour scale.

the tray. The mixing character of the liquid phase is, however, profoundly influenced by the scale, as has been emphasized above.

HYDRODYNAMICS OF SIEVE TRAYS WITH CATALYST CONTAINERS

There is a great deal of industrial interest in reactive distillation (Taylor and Krishna, 2000). For heterogeneously

catalysed liquid phase reactions, the liquid phase has to be brought into intimate contact with catalyst particles. Both packed columns (random packed or structured) and tray columns could be used. In order to avoid diffusional limitations, the catalyst particles have to be smaller than about 3 mm in size. Such catalyst particles are usually encased within wire-gauze envelopes as in the KATAPAK-S and KATAMAX constructions of Sulzer Chemtech and Koch-Glitsch. An alternative to the KATAPAK-S and KATAMAX construction is to dispose the wire gauze parcels containing
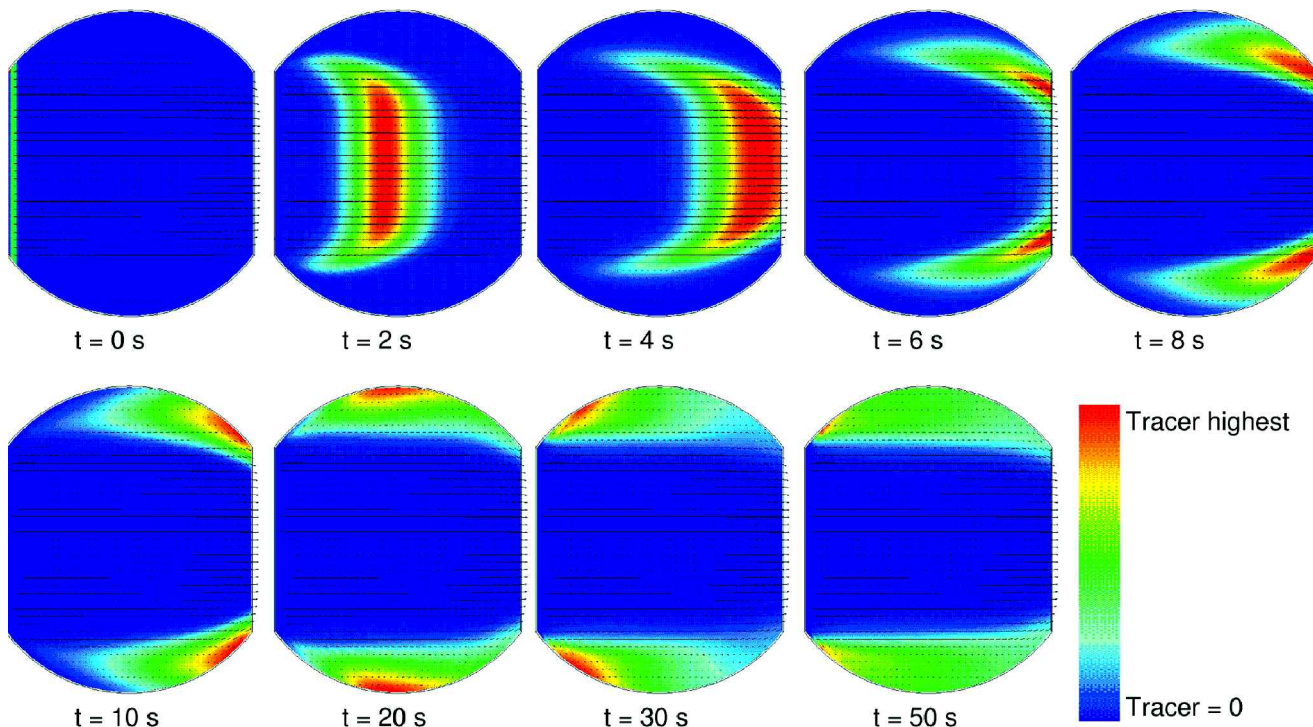
Figure 2. Snapshots showing the movement of colour tracer across the tray. Highest tracer concentration is denoted by red. Blue areas do not contain tracer. The shades of colours in between blue (zero tracer concentration) and red (highest tracer concentration) denote the tracer concentrations.
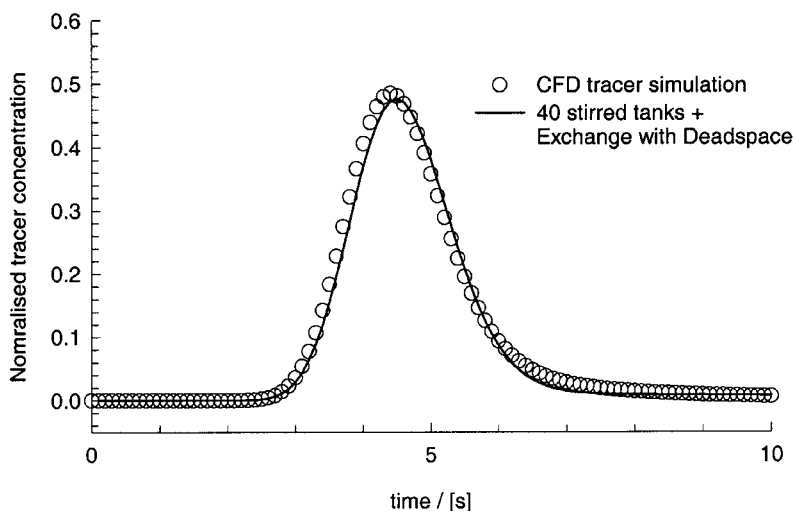
Figure 3. Residence time distribution obtained from pulse tracer injection CFD experiment shown in Figure 2. The open circles represent the results of CFD simulations. The continuous lines represent the response calculated from a model with *N* stirred tanks in series, including exchange with a dead zone.
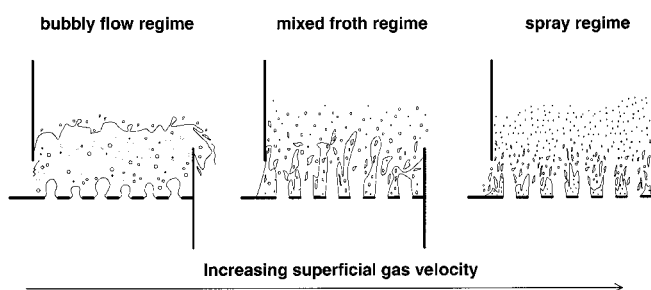

Figure 4. Flow regimes on sieve tray.

catalyst along the liquid flow direction of a sieve tray distillation column as shown in Figure 16. The liquid hold-up is usually much higher in sieve tray columns as compared to packed columns and this is an advantage when carrying out relatively slow, catalysed, liquid phase reactions. A further advantage of a catalytic sieve tray construction is that the contacting on any tray is *cross-current* and for large diameter columns there will be a high degree of

staging in the liquid phase; this is advantageous from the point of view of selectivity and conversion. There is very little published information on the hydrodynamics of such contacting devices. CFD simulations are particularly suited to describe the hydrodynamics, because the preferred regime of operation in reactive distillation tray columns is the bubbly flow regime, which is well described in CFD, as seen in the foregoing.
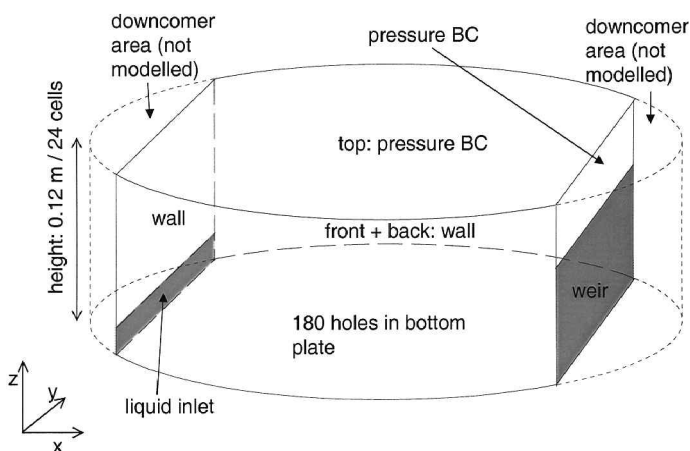
Figure 5. Specification of the computational space used in the CFD simulations. Total cross-sectional area of column = 0.07068 m²; downcomer area = 0.003675 m²; active bubbling area = 0.063 m²; total number of holes = 180; hole area = 0.00414 m²; fractional hole area to bubbling area = 6.54%.
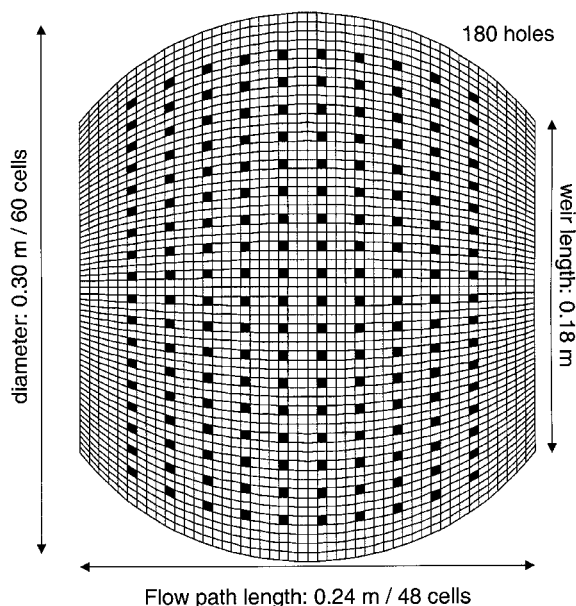
Figure 6. Layout of the distributor plate used in the CFD simulations: total number of holes = 180; hole area = 0.00414 m^2; fractional hole area to bubbling area = 6.54%. The average area of one hole is 23 mm^2.

The gas–liquid flow in the open spaces between the catalyst containers can be modelled in exactly the same manner as before (van Baten *et al.*, 2001a,b). When viewed from the front, the hydrodynamics has the same chaotic character as before (see Figure 7), as is evidenced in the snapshot shown in Figure 17(a). There tends to be accumulation of liquid on top of the catalyst containers; this is evidenced by the snapshot taken from the front, at a position 25 mm off-centre; see Figure 17(b).

The liquid accumulation is clearly evident in the snapshot taken from the weir view; see Figure 17(c). The profiles of liquid holdup along the tray dispersion height shown in Figure 18, show clear differences with the corresponding simulations without containers shown in Figure 11. In practice, this liquid accumulation can be prevented by tapering the top of the containers.

The presence of the liquid containers tends to dampen out the circulation cells and the flow along from the inlet to the weir has a more plug flow character; this is evidenced by the top view snapshot shown in Figure 19.

Good quantitative agreement between the CFD simulation results with catalyst containers and experimental results of Van Baten *et al.* (2001a,b) as is evidenced in the comparison presented in Figure 20. The experiments have been performed in a rectangular tray rather than in a round tray (see http://ct-cr4.chem.uva.nl/kattray/).
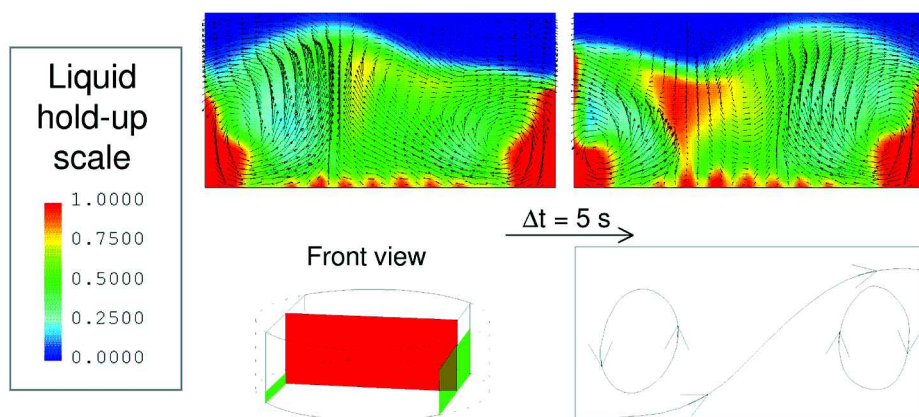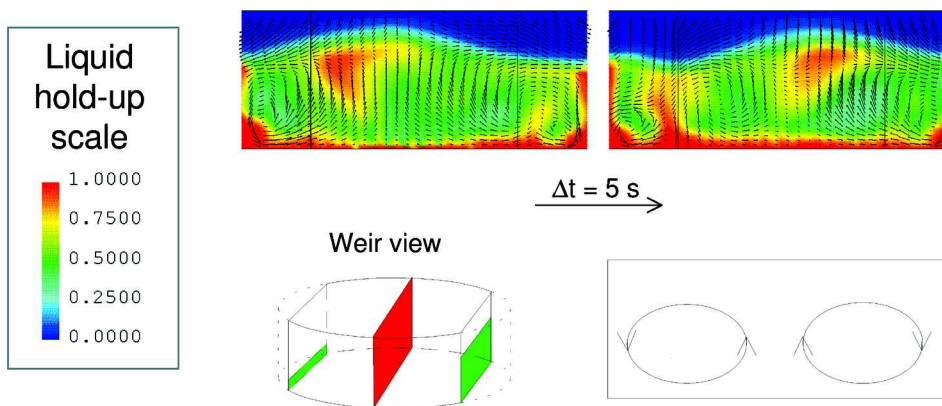

Figure 7. Snapshots of the front view of 0.3 m sieve tray simulations at a superficial gas velocity, $U_G = 0.7\,\mathrm{m\,s^{-1}}$; weir height $h_w = 80$ mm; liquid weir load $Q_L/W = 8.25 \times 10^{-4}\,\mathrm{m^3\,s^{-1}\,m^{-1}}$. The colours indicate the liquid holdup (scale on the left).

Figure 8. Snapshots of the weir view of 0.3 m sieve tray simulations at a superficial gas velocity, $U_G = 0.7\,\mathrm{m\,s^{-1}}$; weir height $h_w = 80$ mm; liquid weir load $Q_L/W = 8.25 \times 10^{-4}\,\mathrm{m^3\,s^{-1}\,m^{-1}}$. The colours indicate the liquid holdup (scale on the left).

top view: 10 mm

liquid holdup scale:

1.0000
0.7500
0.5000
0.2500
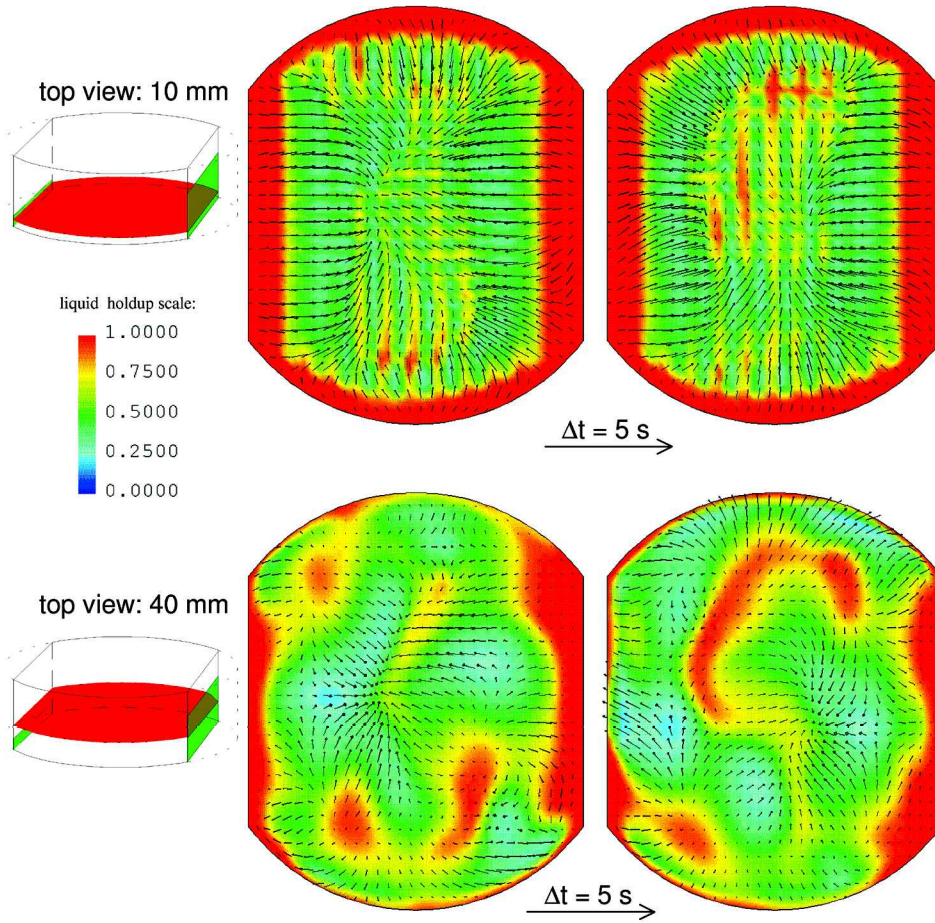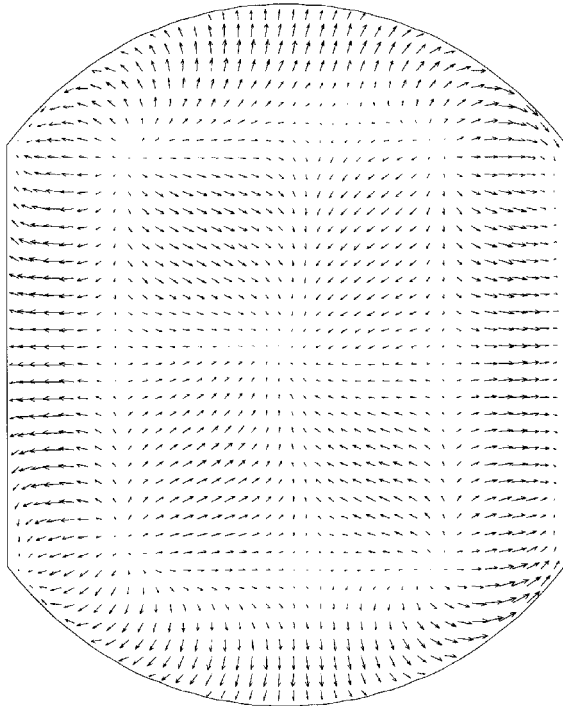0.0000

$\Delta t = 5$ s

top view: 40 mm

$\Delta t = 5$ s

Figure 9. Snapshots of the top views, 10 and 40 mm above the floor of the 0.3 m tray. Superficial gas velocity, $U_G = 0.7$ m s^{-1}; weir height $h_w = 80$ mm; liquid weir load $Q_L/W = 8.25 \times 10^{-4}$ m^3 s^{-1} m^{-1}. The colours indicate the liquid holdup (scale on the left).

Figure 10. Time-averaged liquid phase velocity vectors, 40 mm above the floor of the 0.3 m tray. Superficial gas velocity, $U_G = 0.7$ m s^{-1}; weir height $h_w = 80$ mm; liquid weir load $Q_L/W = 8.25 \times 10^{-4}$ m^3 s^{-1} m^{-1}.
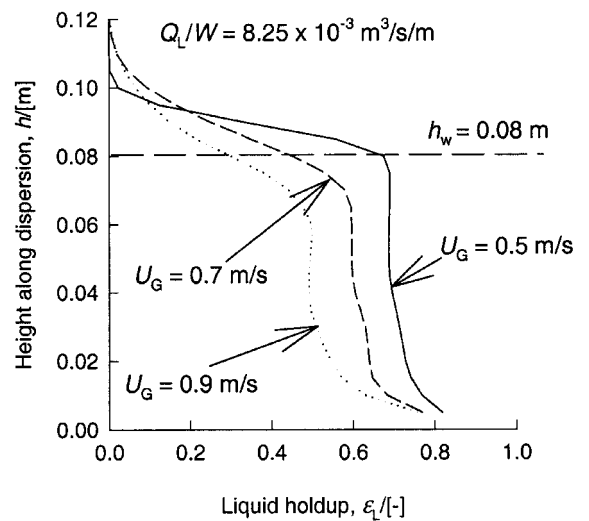
Figure 11. Distribution of liquid holdup along the height of the dispersion for superficial gas velocities, $U_G = 0.5$, 0.7 and 0.9 m s^{-1}. Weir height $h_w = 80$ mm; liquid weir load $Q_L/W = 8.25 \times 10^{-4}$ m^3 s^{-1} m^{-1}. The values of the holdup are obtained after averaging along the x- and y-directions and over a sufficiently long time interval once quasi-steady-state-conditions are established.
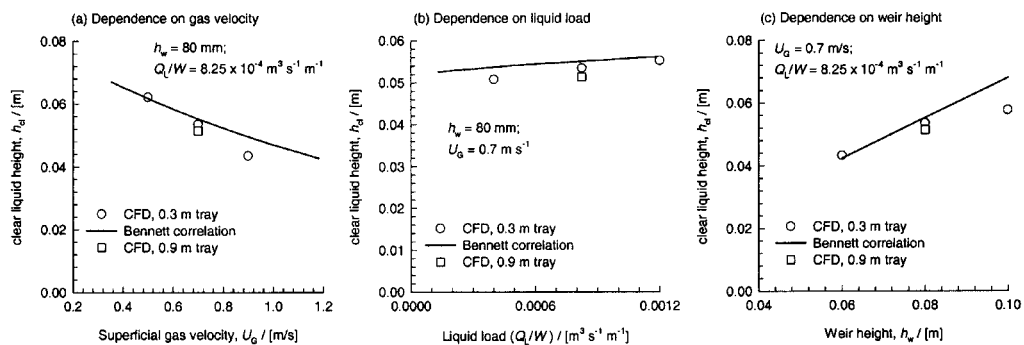
Figure 12. Clear liquid height as a function of the (a) superficial gas velocity, (b) liquid load, and (c) weir height. Comparison of Bennett correlation with CFD simulations for 0.3 m diameter tray. Also shown are CFD simulation results for 0.9 m tray (see below).
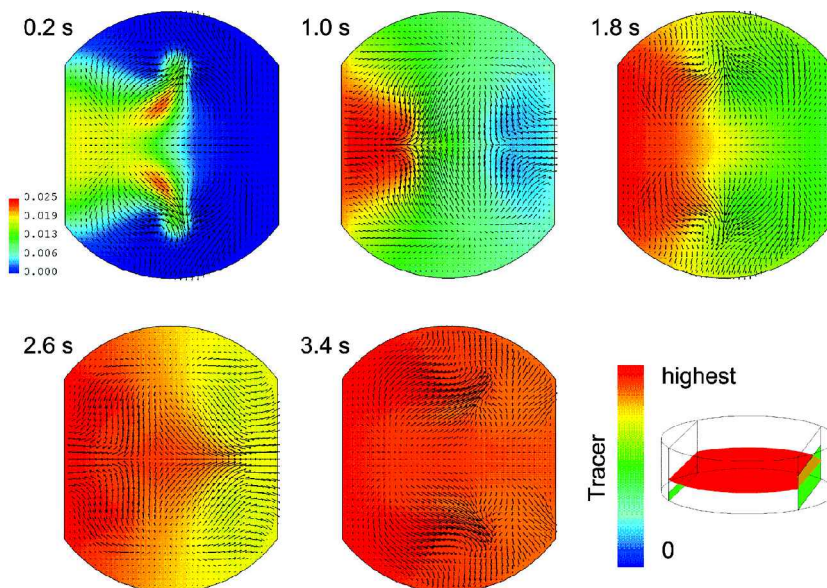

Figure 13. Snapshots of tracer concentration at various times after tracer injection, viewed from the top at 40 mm above the floor of the 0.3 m tray. Superficial gas velocity, $U_G = 0.7 \, \text{m s}^{-1}$; weir height $h_w = 80 \, \text{mm}$; liquid weir load $Q_L/W = 8.25 \times 10^{-4} \, \text{m}^3 \, \text{s}^{-1} \, \text{m}^{-1}$. The colours indicate the liquid tracer concentration (see scale). Further computational details of the algorithms used, boundary conditions, including animations, are available on our web site (http://ct-cr4.chem.uva.nl/sievetrayCFD/tracer/).
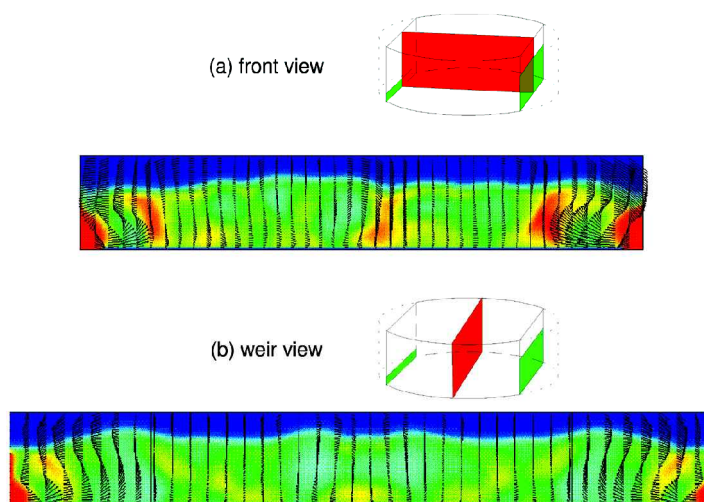

Figure 14. Snapshots of the (a) front view and (b) weir view of 0.9 m sieve tray simulation at a superficial gas velocity. $U_G = 0.7 \, \text{m s}^{-1}$; weir height $h_w = 80 \, \text{mm}$; liquid weir load $Q_L/W = 8.25 \times 10^{-4} \, \text{m}^3 \, \text{s}^{-1} \, \text{m}^{-1}$. The colours indicate the liquid holdup (scale as in Figure 7). Further computational details of the algorithms used, boundary conditions, including animations are available on our web site (http://ct-cr4.chem.uva.nl/sievetrayCFD/big/).
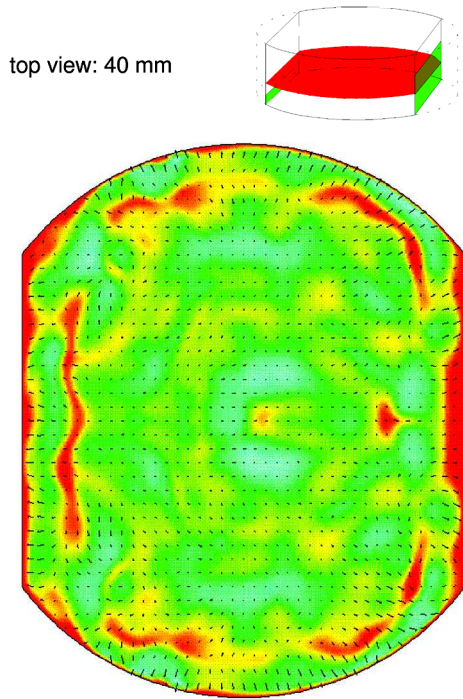
top view: 40 mm

Figure 15. Snapshots of the top view, 40 mm above the tray floor, of 0.9 m sieve tray simulation at a superficial gas velocity. $U_G = 0.7\,\text{m s}^{-1}$; weir height $h_w = 80\,\text{mm}$; liquid weir load $Q_L/W = 8.25 \times 10^{-4}\,\text{m}^3\,\text{s}^{-1}\,\text{m}^{-1}$. The colours indicate the liquid holdup (scale as in Figure 7). See also our web site (http://ct-cr4.chem.uva.nl/sievetrayCFD/big/).

(a) front view: centre

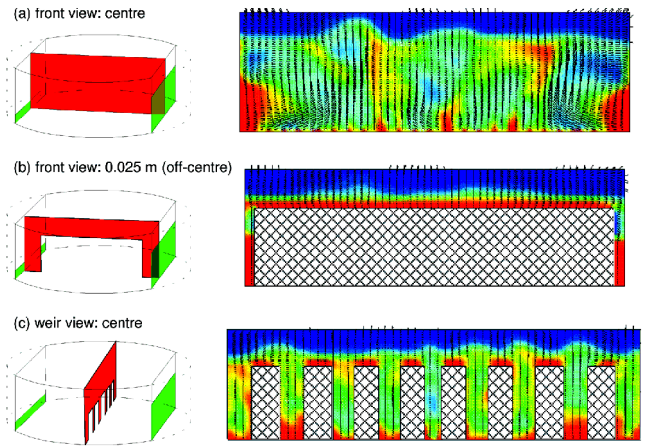(b) front view: 0.025 m (off-centre)

(c) weir view: centre

Figure 17. (a) Snapshots of the front view, (b) off-centre front view and (c) weir view of 0.3 m catalyst containing sieve tray simulations at a superficial gas velocity. $U_G = 0.7\,\text{m s}^{-1}$; weir height $h_w = 80\,\text{mm}$; liquid weir load $Q_L/W = 8.25 \times 10^{-4}\,\text{m}^3\,\text{s}^{-1}\,\text{m}^{-1}$. The colours indicate the liquid holdup (scale as in Figure 7). Animations can be viewed on our web site (http://ct-cr4.chem.uva.nl/katsievetrayCFD/).
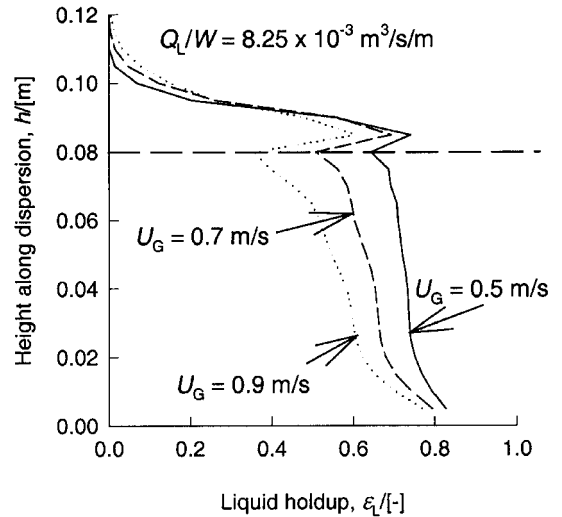

Figure 18. Simulation results with catalyst containers. Distribution of liquid holdup along the height of the dispersion for superficial gas velocities. $U_G = 0.5$, 0.7 and $0.9\,\text{m s}^{-1}$, weir height $h_w = 80\,\text{mm}$; liquid weir load $Q_L/W = 8.25 \times 10^{-4}\,\text{m}^3\,\text{s}^{-1}\,\text{m}^{-1}$. The corresponding simulation results without catalyst containers are shown in Figure 11.
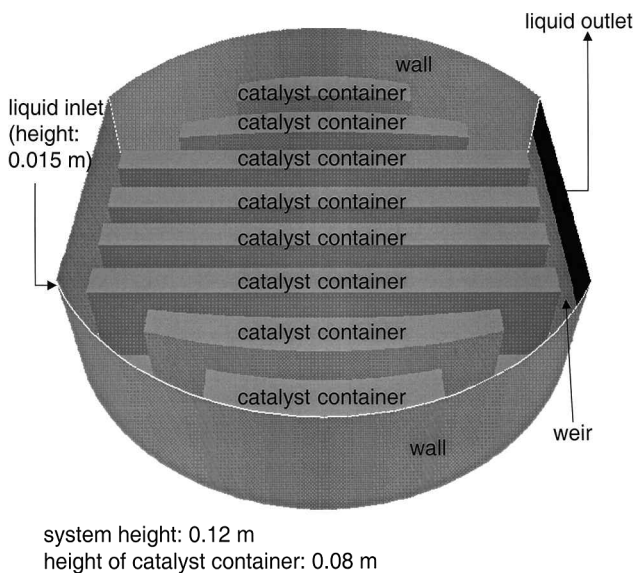

Figure 16. Computational space for CFD simulations 0.3 m diameter sieve tray containing catalyst-filled containers.
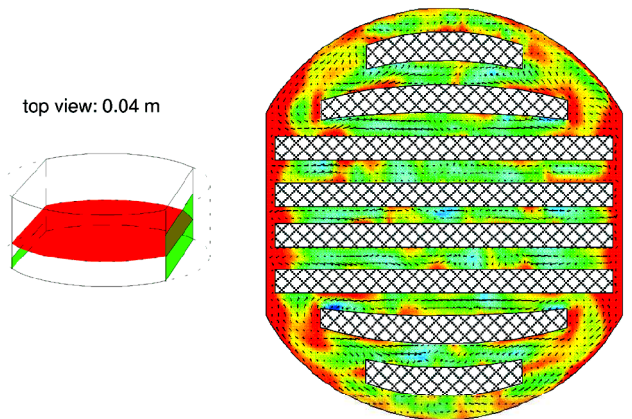
top view: 0.04 m

Figure 19. Snapshots of the top view of 0.3 m catalyst containing sieve tray simulations. Operating conditions as in legend to Figure 17.
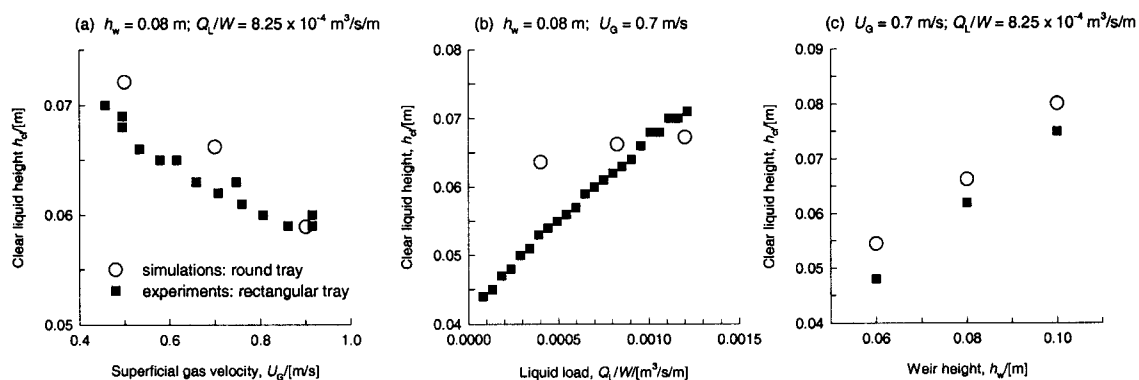
Figure 20. Experiments vs CFD simulations for hydrodynamics of sieve trays with catalyst containers. Clear liquid height as a function of the (a) superficial gas velocity, (b) liquid load, and (c) weir height. The experiments have been performed in a rectangular tray rather than in a round tray (see http://ct-cr4.chem.uva.nl/kattray/).

CONCLUSIONS

We have discussed the modelling of the sieve tray hydrodynamics using CFD. Approaches, neglecting the gas phase and assuming the flow to be two-dimensional in character exaggerate the importance of dead zones. A fully three-dimensional transient simulation reveals the true three-dimensional and chaotic character with liquid circulation cells in both vertical and horizontal directions. The predictions of the clear liquid height and liquid hold-up from the CFD simulations show the right trends with varying superficial gas velocity, liquid weir load and weir height, and match the values of the Bennett *et al.* (1983) correlation quite closely. The existence of dead zones is unlikely in actual practice. CFD simulations are able to describe the changes in the hydrodynamics with increasing scale. Comparing of the simulations of the 0.3 and 0.9 m diameter trays shows that the number of circulating cells increases with column diameter. This means that the liquid phase will tend to have a plug flow character in large diameter trays. The column diameter has, however, a small effect on the clear liquid height and gas holdup on the tray.

CFD simulations are particularly helpful in describing the hydrodynamics of sieve trays containing internals such as catalyst containing envelopes.

Our studies show that CFD simulations can be a powerful investigative, and design tool for distillation trays. The success of the CFD technique is so far restricted to the bubbly flow regime. To describe the spray regime, more reliable models to represent the interphase drag coefficient will be required. This area requires further attention.

NOMENCLATURE

d_G	diameter of gas bubble, m
C	parameter used in the Bennett correlation (17)
C_D	drag coefficient, dimensionless
g	acceleration due to gravity, $9.81\,\mathrm{m\,s^{-2}}$
$\mathbf{g}$	acceleration vector due to gravity
h_{cl}	clear liquid height, m
h_w	weir height, m
h	position along height, m
$\mathbf{M}$	interphase momentum exchange term, $\mathrm{N\,m^{-3}}$
p	pressure, $\mathrm{N\,m^{-2}}$
Q_L	liquid flow rate across tray, $\mathrm{m^3\,s^{-1}}$
Re	Reynolds number, dimensionless
t	time, s

$\mathbf{u}$	velocity vector, $\mathrm{m\,s^{-1}}$
U_G	superficial gas velocity, $\mathrm{m\,s^{-1}}$
V_{slip}	slip velocity between gas and liquid, $\mathrm{m\,s^{-1}}$
W	weir length, m
x	coordinate, m
y	coordinate, m
z	coordinate, m

Greek symbols

ε	volume fraction of phase, dimensionless
μ	viscosity of phase, $\mathrm{Pa\,s}$
ρ	density of phases, $\mathrm{kg\,m^{-3}}$

Subscripts

cl	clear liquid
G	referring to gas phase
k	index referring to one of the phases
L	referring to liquid phase
slip	slip

Superscripts

B	from Bennett correlation

REFERENCES

Bennett, D.L., Agrawal, R. and Cook, P.J., 1983, New pressure drop correlation for sieve tray distillation columns, *AIChE J*, 29: 434–442.

Borchersger, O., Busch, C., Sokolichin, A. and Eigenberger, G., 1999, Applicability of the standard κ–ε turbulence model to the dynamic simulation of bubble columns: part II: comparison of detailed experiments and flow simulations, *Chem Engng Sci*, 54: 5927–5935.

Hofhuis, P.A.M. and Zuiderweg, F.J., 1979, Sieve plates: dispersion density and flow regimes, *Inst Chem Engrs Symp Ser*, 56: 2.2/1–2.2/26.

Jakobsen, H.A., Sannæs, B.H., Grevskott, S. and Svendsen, H.F., 1997, Modeling of bubble driven vertical flows, *Ind Engng Chem Res*, 36: 4052–4074.

Kister, H.Z., 1992, *Distillation Design* (McGraw-Hill, New York, USA).

Krishna, R. and Van Baten, J.M., 1999, Simulating the motion of gas bubbles in a liquid, *Nature*, 398: 208.

Krishna, R. and Van Baten, J.M., 2001a, Scaling up bubble column reactors with the aid of CFD, *Trans IChemE Part A*, *Chem Eng Res Des*, 79: 283–309.

Krishna, R. and Van Baten, J.M., 2001b, Using CFD for scaling up gas–solid bubbling fluidised bed reactors with Geldart A powders, *Chem Engng J*, 82: 247–257.

Krishna, R., Van Baten, J.M., Ellenberger, J., Higler, A.P. and Taylor, R., 1999, CFD simulations of sieve tray hydrodynamics, *Trans IChemE Part A*, *Chem Eng Res Des*, 77: 639–646.

Krishna, R., Van Baten, J.M., Urseanu, M.I. and Ellenberger, J., 2000a, Rise velocity of single circular-cap bubbles in two-dimensional beds of powders and liquids, *Chem Engng Process*, 39: 433–440.

Krishna, R., Van Baten, J.M. and Urseanu, M.I., 2000b, Three-phase Eulerian simulations of bubble column reactors operating in the churn-turbulent flow regime: a scale up strategy, *Chem Engng Sci*, 55: 3275–3286.

Launder, B.E. and Sharma, B.T., 1974, Application of the energy dissipation model of turbulence to the calculation of flow near a spinning disc, *Lett Heat Mass Transfer*, 1: 131–138.

Liu, C.J., Yuan, X.G., Yu, K.T. and Zhu, X.J., 2000, A fluid dynamic model for flow-pattern on distillation tray, *Chem Engng Sci*, 55: 2287–2294.

Lockett, M.J., 1986, *Distillation Tray Fundamentals* (Cambridge University Press, Cambridge, UK).

Mehta, B., Chuang, K.T. and Nandakumar, K., 1998, Model for liquid phase flow on sieve trays, *Trans IChemE Part A, Chem Eng Res Des*, 76: 843–848.

Porter, K.E., Lockett, M.J. and Lim, C.T., 1972, The effect of liquid channelling on distillation plate efficiency, *Trans IChemE*, 45: 91–101.

Rhie, C.M. and Chow, W.L., 1983, Numerical study of the turbulent flow past an airfoil with trailing edge separation, *AIAA J*, 21: 1525–1532.

Stichlmair, J.G. and Fair, J.R., 1998, *Distillation Principles and Practice* (Wiley-VCH, New York).

Taylor, R. and Krishna, R., 2000, Modelling reactive distillation, *Chem Engng Sci*, 55: 5183–5229.

Van Baten, J.M. and Krishna, R., 2000, Modelling of sieve tray hydraulics using computational fluid dynamics, *Chem Engng J*, 77: 143–152.

Van Baten, J.M., Ellenberger, J. and Krishna, R., 2001a, Hydrodynamics of reactive distillation tray column with catalyst containing envelopes: experiments vs CFD simulations, *Catal Today*, 66: 233–240.

Van Baten, J.M., Ellenberger, J. and Krishna, R., 2001b, Hydrodynamics of distillation tray column with structured catalyst containing envelopes: experiments vs CFD simulations, *Chem Engng Technol*, 24: 077–1081.

Van Doormal, J. and Raithby, G.D., 1984, Enhancement of the SIMPLE method for predicting incompressible flows, *Numer Heat Transfer*, 7: 147–163.

Van Wachem, B.G.M., Schouten, J.C., van den Bleek, C.M., Krishna, R. and Sinclair, J.L., 2001, Comparative analysis of CFD models for dense gas–solid systems, *AIChE J*, 47: 1035–1051.

Zuiderweg, F.J., 1982, Sieve trays. A view on the state of the art, *Chem Engng Sci*, 37: 1441–1464.

ACKNOWLEDGEMENT

ADDRESS

Correspondence concerning this paper should be addressed to Professor R. Krishna, Department of Chemical Engineering, University of Amsterdam, Nieuwe Achtergracht 166, 1018 WV Amsterdam, The Netherlands. E-mail: krishna@science.uva.nl